Simulations of Viscoelastic Ink Droplet Ejections Using the Finite Difference Level Set Method and Equivalent Circuit

Jiun-Der Yu* *and Shinri Sakai***

** Epson Research and Development, Inc., San Jose, CA, U. S. A.*

*** Seiko Epson Corporation, Fujimi-machi, Suwa-gun, Nagano, 399-0293 Japan*

Abstract

We developed a coupled finite difference level set projection code for the simulation of viscoelastic ink droplet ejections. The ink is modeled by the Oldroyd-B viscoelastic fluid model, which is decent for dilute polymer solutions, while the air is modeled as a Newtonian fluid. A slipping contact line model was implemented to resolve the contradiction of the moving contact line and the no-slip condition. For practical applications, the code was connected to an equivalent circuit, which simulates the interior ink flow considering the influence of ink cartridge, vibration plate, and PZT actuator. Simulation examples showing the effect of fluid elasticity will be presented.

Introduction

Piezoelectric drop-on-demand ink jet print heads require a long development cycle to meet design goals. To speed up the process, numerical simulations of the droplet ejection process are very helpful. A practical ink-jet simulation may be carried out by connecting a computational fluid dynamics (CFD) code to an equivalent circuit, as shown in Figure 1. As explained in [1, 2], an equivalent circuit receives as an input the dynamic voltage applied to the piezoelectric PZT actuator and simulates the interior ink flow under the influence of the ink cartridge, supply channel, vibration plate, and actuator. It calculates an inflow pressure to the ink jet nozzle to drive the CFD code. The CFD code then solves the incompressible two-phase flow equations for fluid velocity, pressure and interface position, and feeds back the ink flow rate to the equivalent circuit. The sequence is repeated as long as needed.

In recent years, ink jet technologies have found applications other than the desktop printer. These involve such areas as microdispensing of bioactive fluids through high throughput injection devices, creation of cell attachment sites, scaffolds for tissue engineering, coatings and drug delivery systems for controlled drug release, blood flow past valves, and other industrial printing applications. Due to the existence of long polymer fibers or big organic molecules, inks used in these new applications are usually viscoelastic, i.e. the relation between the stress tensor and the rate of deformation tensor at an instant depends on the deformation history.

One of the most perplexing problems in viscoelastic flow is the limitations on the Weissenberg number. Algorithms typically go unstable for a moderate range of Weissenberg numbers, and this has been the subject of considerable research: large stress levels, coupled to regimes of rapid changes are computationally difficult and cause many schemes, both finite difference and finite element, to go unstable. An excellent introductory review of the mathematical and numerical issues may be found in [3].

In previous works [1, 4, 5], we have built coupled level set projection methods for the ink jet process of Newtonian fluids on rectangular and arbitrary quadrilateral grids. In this work, we extend these techniques to the viscoelastic regime. Our coupled finite difference algorithm seamlessly incorporates: (1) a projection method to enforce the fluid incompressibility; (2) the level set methods to implicitly capture the moving interface; (3) a higher-order Godunov type algorithm for the convection terms in the momentum and level set equations; (4) a simple first-order upwind algorithm for the convection term in the viscoelastic stress equations; (5) the central difference for viscosity, surface tension, and other upper-convected derivative terms; and (6) an equivalent circuit to calculate the inflow pressure (or flow rate) with given dynamic voltage.

We apply these techniques to simulate the droplet ejection process under a range of viscoelastic relaxation parameters. Our results demonstrate that the ink elasticity has a dramatic effect on droplet ejection and formation. For Newtonian fluids under reasonable configurations and parameters, pressure bursts in the ink chamber expel ink through the nozzle which then pinches off and breaks into droplets. As the ink characteristics become more viscoelastic, droplets become longer in shape, smaller in volume, and pinch off later. In the case of larger viscoelastic relaxation times, droplets are pulled back by the combination of elastic effects and surface tension and cannot be ejected.

Governing Equations

Since the nozzle geometry is axisymmetric, we adopt the axisymmetric coordinate system (see Figure 3) and consider velocity field $\mathbf{u} = u(r,z)\mathbf{e}_r + v(r,z)\mathbf{e}_z$. We employ the level set method[6] to capture the ink-air interface. The level set, which is initialized as the signed distance to the interface, is defined by

$$\phi(r,z,t)\begin{cases} <0 & \text{if} \quad (r,z)\in \text{fluid 2 (air)} \\ =0 & \text{if} \quad (r,z)\in \text{interface} \\ >0 & \text{if} \quad (r,z)\in \text{fluid 1 (ink)} \end{cases} . \tag{1}$$

The governing equations for two-phase (ink and air) incompressible flows consist of the continuity equation

$$\nabla\cdot\mathbf{u} = 0 , \tag{2}$$

the momentum equations

$$\frac{D\mathbf{u}}{Dt} = -\frac{\nabla p}{\rho(\phi)} + \frac{\nabla\cdot(2\mu(\phi)\mathbf{D})}{\rho(\phi)Re} - \frac{\kappa(\phi)\delta(\phi)\nabla\phi}{\rho(\phi)We} + \nabla\cdot\tau , \tag{3}$$

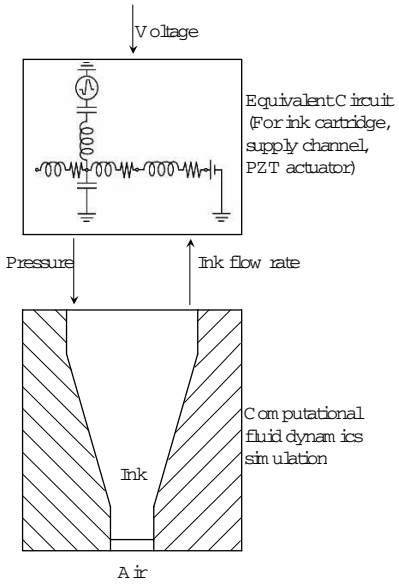

Figure 1. *Connection of a CFD code to an equivalent circuit.*

the viscoelastic stress equations

$$\frac{D\tau}{Dt} = \tau\cdot(\nabla\mathbf{u}) + (\nabla\mathbf{u})^T\cdot\tau - \frac{1}{\lambda(\phi)}\left(\tau - 2\frac{\mu_p(\phi)}{Re_p}\mathbf{D}\right) , \quad (4)$$

and the level set convection equation

$$\frac{\partial\phi}{\partial t} + \mathbf{u}\cdot\nabla\phi = 0 . \quad (5)$$

In the above, $\frac{D}{Dt} = \frac{\partial}{\partial t} + (\mathbf{u}\cdot\nabla)$ is the Lagrangian time derivative, $\mathbf{D} = \frac{1}{2}[\nabla\mathbf{u} + (\nabla\mathbf{u})^T]$ the rate of deformation tensor, p the pressure, τ the viscoelastic stress tensor, δ the Dirac delta function, and $\kappa(\phi) = \nabla\cdot(\frac{\nabla\phi}{|\nabla\phi|})|_{\phi=0}$ the curvature. The density and viscosity ratios, normalized relaxation time, solute viscosity, Reynolds numbers of the solvent and solute, and Weber number are defined by

$$\begin{aligned}
\rho(\phi) &= \begin{cases} 1 & \text{if } \phi \geq 0 \\ \rho_2/\rho_1 & \text{if } \phi < 0 \end{cases} , & Re &= \frac{\rho_1 UL}{\mu_1} , \\
\mu(\phi) &= \begin{cases} 1 & \text{if } \phi \geq 0 \\ \mu_2/\mu_1 & \text{if } \phi < 0 \end{cases} , & Re_p &= \frac{\rho_1 UL}{\mu_{p1}} , \\
\lambda(\phi) &= \begin{cases} \lambda & \text{if } \phi \geq 0 \\ 0 & \text{if } \phi < 0 \end{cases} , & We &= \frac{\rho_1 U^2 L}{\sigma} , \\
\mu_p(\phi) &= \begin{cases} \mu_{p1}/\mu_1 & \text{if } \phi \geq 0 \\ 0 & \text{if } \phi < 0 \end{cases} ,
\end{aligned} \quad (6)$$

where σ is the surface tension coefficient, ρ_i the density of the ith fluid, μ_i the dynamic viscosity of the ith fluid, λ the relaxation time of the 1st fluid (ink), μ_{p1} the solute dynamic viscosity, U the velocity scale, and L the length scale.

The no-slip condition for viscous fluid is enforced at solid nozzle wall. At nozzle inflow and outflow, our formulation allows us to prescribe either the velocity or the pressure. Boundary conditions for the viscoelastic stresses, when needed, are implemented using a zeroth-order extrapolation.

We would like to make several comments. First, since the second fluid is assumed to be the air, which is Newtonian, the viscoelastic stress tensor τ vanishes in fluid #2. The dynamic viscosity μ_1 is actually the dynamic viscosity of the ink solvent, which is usually water. Second, equation (4) together with the viscosity term in the momentum equations constitutes the Oldroyd-B viscoelastic fluid model. The first three terms together in (4) constitute the upper-convected time derivative of the viscoelastic stress tensor. Third, because the size of typical ink jet print heads is small, the gravity term is not important and is omitted. The inclusion of a gravity term does not change any part of the numerical schemes described in the next sections. Finally, the numerical schemes work equally well for cases in which both fluids are viscoelastic.

Contact Model and Equivalent circuit

Because the no-slip condition contradicts the fact that the contact point keeps sliding on the nozzle wall in droplet ejection, we need a contact model to resolve the problem[1]. We first define the contact angle θ as the angle made by the ink-air interface and the solid, measured from the side of ink. The advancing critical contact angle θ_a and receding critical contact angle θ_r are the maximum and minimum contact angles for the contact point to stay. In most situations $\theta_r < \theta_a$. Actual values of θ_a and θ_r depend on both the fluids and the solid surface. The triple point is allowed to move toward the air (ink) side if $\theta \geq \theta_a (\leq \theta_r)$ and is not allowed to move otherwise. If the triple point is allowed to move, the no-slip condition in a close vicinity of the triple point is switched to the free slip condition. In this work, we chose to set two cells at each side of the contact point to free slip should the triple point be allowed to move.

For ink jet simulations, one needs to prescribe a velocity or pressure at the nozzle inflow. However, only the input voltage to the PZT is known. An equivalent circuit model can be used to solve the problem. The ink flow rate and pressure are first taken as dependent variables. Each component of the ink jet print head, such as the nozzle, pressure chamber, vibration plate, PZT actuator, and ink cartridge, is expressed in terms of the compliance and acoustic resistance. These acoustics elements are finally transferred to their equivalent inductance, capacitance, and electric resistance to form an equivalent circuit. By solving the equivalent circuit and the flow equations in turn, one simulates a real ink jet.

The particular equivalent circuit we used is not described here; readers are referred to Sakai[2] for an introduction to print head structures and equivalent circuits. A typical inflow pressure is shown in Figure 2. The pressure pattern contains a high frequency signal. It is basically the fundamental natural frequency of the system, which is several times higher than the driving voltage frequency in this case.

Numerical Algorithm

Suppose we know quantities $\mathbf{u}^n, \tau^n, p^n, \phi^n$, the purpose of an algorithm is to obtain $\mathbf{u}^{n+1}, \tau^{n+1}, p^{n+1}, \phi^{n+1}$. The following algorithm is 1st-order accurate in time.

A. Level set update

The level set is updated by

$$\phi^{n+1} = \phi^n - \Delta t\,[\mathbf{u}\cdot\nabla\phi]^{n+1/2} . \quad (7)$$

A second-order explicit Godunov scheme is applied for the time-centered advection term $[\mathbf{u}\cdot\nabla\phi]^{n+1/2}$. Once ϕ^{n+1} is obtained, we calculate $\phi^{n+1/2}=(\phi^n+\phi^{n+1})/2$.

B. Explicit time integration for momentum equations

If the velocity predictor defined by

$$\mathbf{u}^* = \Delta t\left\{\frac{\nabla\cdot[2\mu(\phi^{n+1/2})\mathbf{D}^n]}{\rho(\phi^{n+1/2})Re} - [(\mathbf{u}\cdot\nabla)\mathbf{u}]^{n+1/2} - \frac{[\kappa(\phi)\delta(\phi)\nabla\phi]^{n+1/2}}{\rho(\phi^{n+1/2})We} + \nabla\cdot\tau^n\right\} + \mathbf{u}^n \tag{8}$$

is first calculated, the time-discretized momentum equations can be written as

$$\mathbf{u}^{n+1} = \mathbf{u}^* - \frac{\Delta t}{\rho(\phi^{n+1/2})}\nabla p^{n+1}\ . \tag{9}$$

We apply a second-order explicit Godunov scheme for the advection term and the central difference for the viscosity and surface tension terms in (8). It is noted that the determination of $\mathbf{u}^*$ needs only values at time step n.

C. Projection for $\mathbf{u}^{n+1}$

To enforce the incompressibility condition for time step $n+1$, we apply the divergence operator on both sides of (9). Since $\nabla\cdot\mathbf{u}^{n+1}=0$, we have

$$\nabla\cdot\mathbf{u}^* = \nabla\cdot\left(\frac{\Delta t}{\rho(\phi^{n+1/2})}\nabla p^{n+1}\right)\ . \tag{10}$$

After the pressure p^{n+1} is solved from equation (10), the velocity field $\mathbf{u}^{n+1}$ can be obtained by (9).

D. Mixed algorithm for the viscoelastic stress equations

In the projection step, we obtain both the new pressure and velocity. The time-centered velocity at cell centers can be calculated by $\mathbf{u}^{n+1/2}=(\mathbf{u}^n+\mathbf{u}^{n+1})/2$. We use a mixed algorithm to integrate the viscoelastic stress equations in time:

$$\left(1+\frac{\Delta t}{\lambda_p(\phi^{n+1/2})}\right)\tau^{n+1} = \tau^n + \Delta t\left[\tau^n\cdot(\nabla\mathbf{u}^{n+1/2}) + (\nabla\mathbf{u}^{n+1/2})^T\cdot\tau^n - (\mathbf{u}^{n+1/2}\cdot\nabla)\tau^n\right] + \frac{2\Delta t\mu_p(\phi^{n+1/2})}{\lambda(\phi^{n+1/2})Re_p}\mathbf{D}^{n+1/2}\ . \tag{11}$$

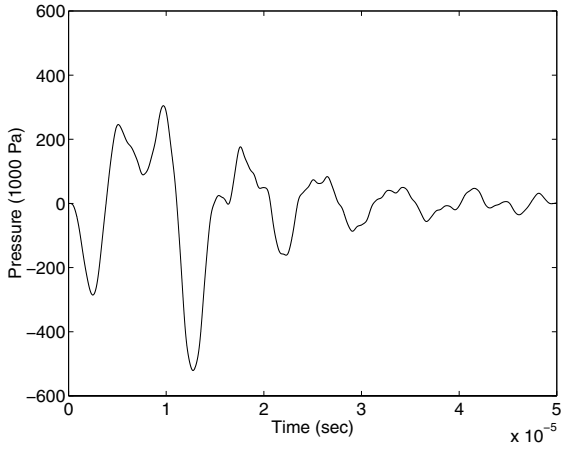

Figure 2. *The typical inflow pressure.*

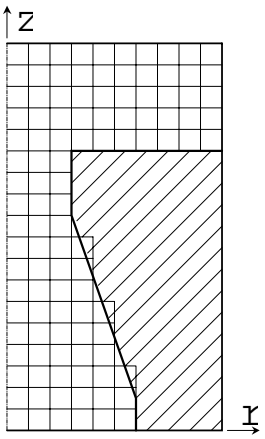

Figure 3. *A typical ink jet nozzle and a rectangular mesh which causes the zig-zag pattern at the shrinking part of nozzle.*

where $\mathbf{u}^{n+1/2}$ is the time-centered velocity field at cell centers. It is noted that the mixed algorithm is explicit on the upper-convected derivative terms and the solute viscosity term, but is implicit on the relaxation term.

Spatial discretization is done on rectangular grids (see Figure 3). Although the rectangular grid results in the zig-zag pattern at the shrinking part of nozzle wall, we found it does not influence simulation results [5]. The meniscus never comes close to the zig-zag portion during droplet ejection. Because of the numerical difficulty caused by the Dirac delta function and by the sharp change of ρ and ν across the free surface, the Heaviside and Dirac delta functions are replaced by smoothed functions (see Yu et al.[4, 5]). The interface thickness is 1.5 grid cells at each side of it.

Numerical example

For an example of droplet ejection simulation, we consider a nozzle (as in Figure 3) of diameter 25μm at the opening and 49.5μm at the bottom. The length of the nozzle opening part, where the diameter is 25μm, is 25μm. The shrinking part of the nozzle is 55μm and the bottom part is 7.5μm. We assumed that the input dynamic voltage has peak voltages at ± 11.15 volts. The corresponding inflow pressure for each simulated cases are very close. The inflow pressure for the Newtonian case is shown in Figure 2. The outflow pressure at the top of the solution domain is set to zero. The solution domain was chosen to be $\{(r,z)|0\le r\le 32.5\mu m,\ 0\le z\le 390\mu m\}$. The advancing and receding critical contact angles are 70° and 20°, respectively. The initial meniscus is assumed to be flat with the nozzle opening. For the purpose of normalization, we chose the nozzle opening diameter (25μm) to be the length scale and 6 m/sec to be the velocity scale. The normalized solution domain is hence $\{(r,z)|0\le r\le 1.25\ , 0\le z\le 15\}$. Since the ink density, solvent and solute dynamic viscosities, and surface tension are approximately $\rho_1 = 1070\ Kg/m^3$, $\mu_1=\mu_{p1}=1.783\times 10^{-3}\ Kg/m\cdot sec$, $\sigma = 0.0396\ Kg/sec^2$, the Reynolds numbers and Weber number are $Re=Re_p=90$, $We=24.3$. Air properties are $\rho_2 = 1.225\ Kg/m^3$, $\mu_2 = 1.77625\times 10^{-3}\ Kg/m\cdot sec$.

Simulation results for Newtonian ink (normalized relaxation time $\lambda=0$) and viscoelastic ink ($\lambda=0.4,1,3$) are plotted in Fig-

ures 4 to 7. It is noted that the major droplet in the last graph of Fig. 4 has already passed the end of the solution domain and hence can not be seen. We see that, although the ink elasticity does not change the inflow pressure by much, it dramatically influences the droplet jettability, pinch off, shape, speed, and size. The droplet pinches off later, becomes longer in shape and smaller in volume, and slows down when the ink elasticity becomes stronger (relaxation time becomes longer). The droplet sizes for the Newtonian case, $\lambda = 0.4$, and $\lambda = 1.0$ are respectively 11.89, 10.98, and 7.66 pico liters. We also found that, at the

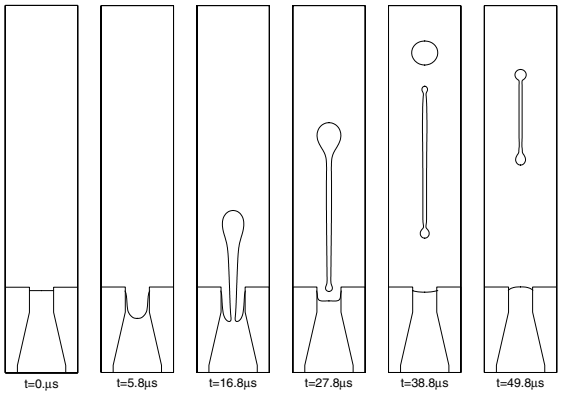

Figure 4. *Droplet ejection (Newtonian, $\lambda = 0$).*

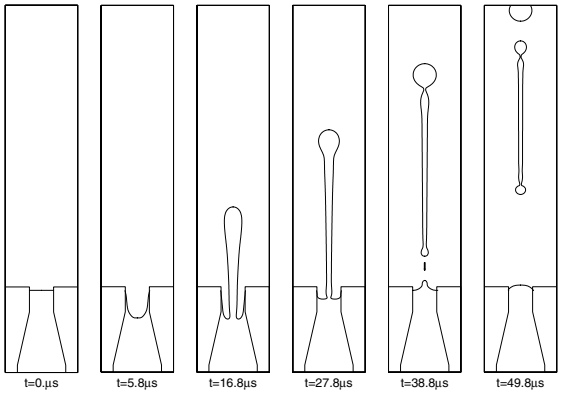

Figure 5. *Viscoelastic ink droplet ejection ($\lambda = 0.4$).*

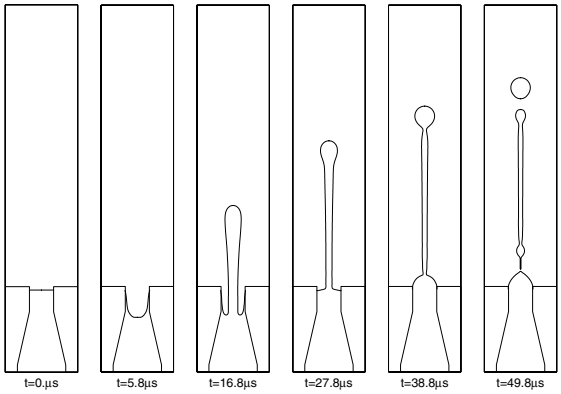

Figure 6. *Viscoelastic ink droplet ejection ($\lambda = 1.0$).*

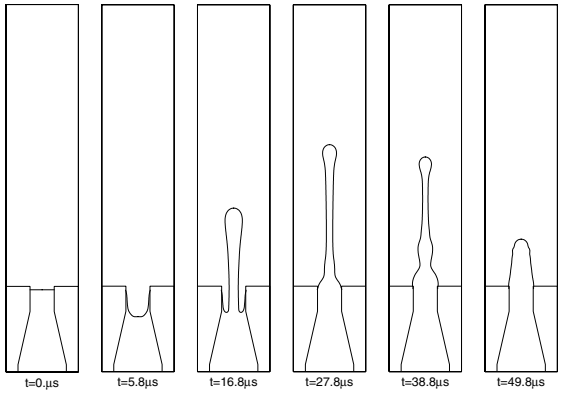

Figure 7. *Viscoelastic ink droplet ejection ($\lambda = 3.0$).*

given peak voltage ($\pm 11.15 volts$) and dynamic pattern, the ink droplet can not be ejected when $\lambda > 1$. In the $\lambda = 3.0$ case, the droplet is at first formed and pushed out, but does not get enough momentum to pinch off. It is finally pulled back by the elastic effect and surface tension. To eject highly viscoelastic ink, one has to either apply higher peak voltage or invent a new dynamic voltage pattern.

References

[1] Jiun-Der Yu and Shinri Sakai, Piezo Ink Jet Simulations Using the Finite Difference Level Set Method and Equivalent Circuit, *Proc. IS&T-NIP19*, pp. 319-322(2003).

[2] Shinri Sakai, Dynamics of Piezoelectric Inkjet Printing Systems. *Proc. IS&T NIP16*, pp. 15-20(2000).

[3] Mark Gerritsma, Time Dependent Numerical Simulations of a Viscoelastic Fluid on a Staggered Grid, PhD thesis, University of Groningen, Netherlands(1996).

[4] Jiun-Der Yu, Shinri Sakai, and James A. Sethian, A Coupled Level Set Projection Method Applied to Ink Jet Simulation, *Interfaces and Free Boundaries*, **5**, pp. 459-482(2003).

[5] Jiun-Der Yu, Shinri Sakai, and James A. Sethian, A coupled Quadrilateral Grid Level Set Projection Method Applied to Ink Jet Simulation, *J. of Comp. Physics*, **206**(1), pp. 227-251(2005).

[6] Stanley Osher and James A. Sethian, Fronts Propagating with Curvature-Dependent Speed: Algorithms Based on Hamilton–Jacobi Formulations, *J. of Comp. Physics*, **79**, pp. 12-49(1988).

Author Biography

Jiun-Der Yu got his PhD from Princeton University in 1995. He is currently the manager of the Device Modeling group of Palo Alto Laboratory, Epson R & D, Inc. Piezo-electro-magnetism, wave propagation, and computational fluid dynamics are his major research interests.

Shinri Sakai is the chief researcher of the OLED Development Center, Seiko Epson Corporation. He received his B.E., M.E., and PhD from Tokyo Institute of Technology, Japan, in 1983, 1985, and 2005 respectively. His primary responsibilities are analysis and computer simulation for ink jet technology and micro liquid process.